GEOPHYSICS, VOL. 71, NO. 5 (SEPTEMBER-OCTOBER 2006); P. B151–B158, 20 FIGS.
10.1190/1.2335636

Rock-property and seismic-attribute analysis of a chert reservoir in the Devonian Thirty-one Formation, west Texas, U.S.A.

Dongjun (Taller) Fu[1], E. Charlotte Sullivan[1], and Kurt J. Marfurt[1]

ABSTRACT

In west Texas, fractured-chert reservoirs of Devonian age have produced more than 700 million barrels of oil. About the same amount of mobile petroleum remains in place. These reservoirs are characterized by microporosity; they are heterogeneous and compartmented, which results in recovery of less than 30% of the oil in place. In this case study the objective was to use cores, petrophysical logs, rock physics, and seismic attributes to characterize porosity and field-scale fractures. The relations among porosity, velocity, and impedance were explored and also reactions among production, impedance, and lineaments observed in 3D attribute volumes. Laboratory core data show that Gassmann's fluid-substitution equation works well for microporous tripolitic chert. Also, laboratry measurements show excellent linear correlation between P-wave impedance and porosity. Volumetric calculations of reflector curvature and seismic inversion of acoustic impedance were combined to infer distribution of lithofacies and fractures and to predict porosity. Statistical relations were established between P-wave velocity and porosity measured from cores, between P-wave impedance and producing zones, and between initial production rates and seismic "fracture lineaments." The strong quantitative correlation between thick-bedded chert lithofacies and seismic impedance was used to map the reservoir. A qualitative inverse relation between the first 12 months of production and curvature lineaments was documented.

INTRODUCTION

Chert is an unconventional reservoir rock that has been developed successfully in west Texas, Oklahoma, California, and Canada (Rogers and Longman, 2001). After 50 years of production, Devonian cherts are still an important petroleum reservoir across the southern Central Basin Platform, in Crane County, Texas (Figure 1). In this case study, cores, petrophysical logs, rock physics, and seismic attributes were used for seismic characterzation of two factors that may exert large influence on production of petrolium: The interwell distribution of porosity and field-scale fractures. In the cherts, the principal zones of porosity are related to distribution of deep-water gravity deposits of carbonate rock. At many localities, these facies are difficult to predict between wells (Ruppel and Barnaby, 2001). Within the survey area, faults are well mapped, particularly along the western margin University Waddell field (Figure 1). More important to production is the distribution of open fractures and small faults that are of subseismic, interwell scale. There discontinuities are rarely evident in cores, but they may be imaged by seismic attributes. In this study, the improvement of resolution of interwell heterogeneity of these chert reservoirs was based on calibration of the relations among porosity, velocity, and impedance and among production, impedance, and lineaments, as observed in 3D attribute volumes. To verify the results, blind tests were used with several wells, for evaluation of the impedance-inversion results, and for comparison of orientations of lineaments with evidence of interwell water breakthrough — which indicate distribution of open fractures.

Understanding the distribution of porosity within a reservoir is critical to exploration for petroleum and for management of reservoirs. Before 3D seismic data were available, cores and well logs were used for correlation and interpolation of porous rock between wells and to extrapolate the distribution of the reservoir beyond the area explainable by information from abundant wells. This method works well if structureal geology and stratigraphy are simple and if wells are "evenly" distributed over the area of interest. However, in many cases, the number of wells is insufficient for sampling of complicated, compartmented reservoirs. For this study, logs from about 150 wells in the University Waddell field were available (Figure 2); the most common log types were gamma ray, neutron, and sonic (Figure 3).

Production data from 66 wells in the University Waddell field were available, and more than 300 m of core. A 14- by 15-km, 3D seismic data volume (Figure 1), permitted the mapping of structural

Manuscript received by the Editor April 15, 2005; revised manuscript received January 16, 2006; published online August 31, 2006.
[1]University of Houston, Allied Geophysical Laboratories, Room 510-Sci & Res Bldg 1, Cullen Road Entrance 14, Houston, Texas 77204. E-mail: dofu@chevron.com; charlotte.sullivan@pnl.gov; kmarfurt@mail.uh.edu.

geology and stratigraphy (Figures 2 and 4), and the documentation of various seismic attributes.

Seismic attributes can provide statistical estimates of reservoir properties, but Kalkomey (1997) warned interpreters to be wary of false-positive correlations. On the basis of Kalkomey's advice, we generated a suite of seismic-attribute cubes. This suite has a well-established sensitivity to reservoir properties of interest: Acoustic impedance to porosity, coherence to faults (Marfurt et al., 1998), reflector curvature to fractures (Roberts, 2001), and coherent energy gradients to lateral variations in tuning thickness (Marfurt, 2006). Given these data, we attempted to define a detailed distribution of the porous chert reservoir facies and of its fluid content. We also attempted to characterize fractures in the chert. The integration of results from these efforts provides us with invaluable information for seismic, log, and core calibration and for reservoir characterization of chert reservoirs in the Permian Basin.

METHODS

Core measurements provided the most detailed, robust estimates of reservoir properties. Logs from more than 300 wells within the survey were the sources of vertically continuous measures of gamma ray intensity, resistivity, and P-wave velocity at vertical resolutions as small as 1 m. Seismic data provide vertical resolution of only 25 m or so, but the 3D reservoir was sampled continuously with 35- by 35-m (110- by 110-ft) bins, which permitted the integration of more detailed measurments from logs and cores, within their appropriate depositional and structural-deformation frameworks. Kallweit and Wood (1982) showed that seismic data can resolve most features that are thicker than one-quarter of the dominant wavelength. They also recognized that in seismic data lateral differences in thickness can be detected that are less than one-quarter of the dominant wavelength. Attributes of 3D seismic data allow the extraction of such subtle, subseismic features on time slices and maps, and thereby permit the interpreter (a) to delineate structural and stratigraphic features of interest, and (b) to link them through depositional and deformational models to well control that is sparse. Twenty-eight samples, from cores of three wells spanned the suite of lithofacies in the Thirtyone Formation, as defined by Ruppel and Hovorka (1995) and by Ruppel and Barnaby (2001). The core descriptions were confirmed, then plugs 2.54 cm (1 inch) in diameter were extracted. The plugs sampled the chert in vertical sections. Plugs were dried. Ends of the plugs were cut for accurate measurement of length and for efficient coupling during measurement of velocity. Bulk density and porosity of 28 samples were measured.

We then selected 11 of the dry samples representing tight and porous facies and measured P- and S- wave velocities. We used the pulse transient method (Hughes and Jones, 1950; Sears and Bonner, 1981), under room temperature and differential pressures that varied from varied from 6.8 Mpa (1000 psi) to 34 Mpa (5000 psi). Each sample was encased in a plastic jacket and sealed with clips; the ends were open. At the ends were a transducer and a receiver; they were coupled with honey paste, for better transmission of signals. The sample- and- transducer system was put in a pressure chamber. Because no fluid was in the samples, confining pressure was equivalent to differential pressure on the sample. An electrical pulse was introduced. From this pulse the first-arrival time of either P- or S-wave signals was recorded. The traveltime and the sample length together permitted calculation of velocities. Uncertainties in measurement of velocities were due mainly to determination of first arrivals, especially of shear waves.

We followed Batzle and Wang (1992) to calculate fluid properties at various temperatures and pressures. We next used Gassmann's (1951) fluid-substitution method to calculate rock properties at simulated reservoir conditions. Finally, we calculated the properties

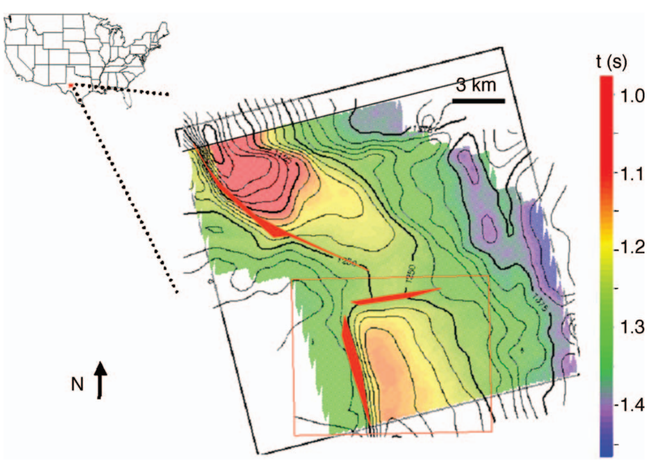

Figure 1. Time-structure map of Devonian Thirtyone Formation, Crane Country, Texas. Two anticlines are shown, each bounded by high-angle reverse faults (red). University Waddell field is shown by red rectangle.

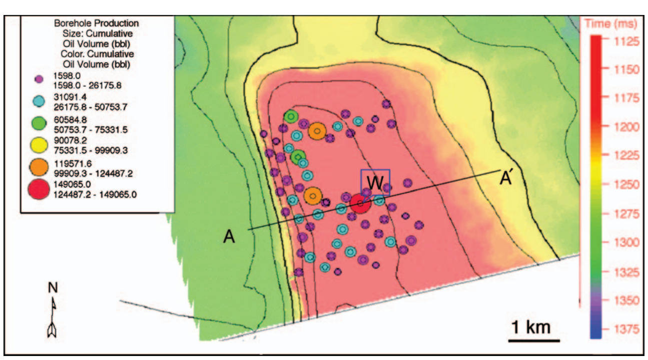

Figure 2. Structural geologic map of Thirtyone Formation, University Waddell field, Crane County, Texas.

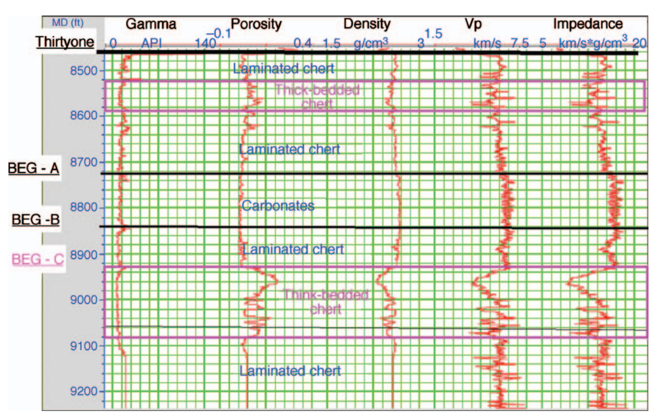

Figure 3. Logs of type well University Waddell field, Crane County, Texas. Location of well shown as "W" in Figure 2. Note that the thick-bedded chert is porous and has a distinctive log signature.

measured by the seismic experiment: density, P- and S-wave velocities, and impedance.

Well logs provided control for the interpretation of the seismic data. Synthetic seismograms were generated for nine wells; statistical wavelets were extracted from traces around each borehole (Figure 3). Synthetic traces (repeated five times) at well "W" (Figure 3) represent a typical seismic-well tie. We picked the Devonian Thirtyone and Frame horizons, which define the top and bottom of Thirtyone Formation, as well as BEG-C marker, which is the top of the main porous chert reservoir (Ruppel and Barnaby, 2001). Although the Thirtyone and Frame horizons were easy to pick, the BEG-C horizon proved to be more difficult to pick because of the variable thickness of the underlying layer (Figure 4).

Acoustic impedance — the product of P-wave velocity and density — is the seismic rock property most successfully linked to porosity (Russell, 1988). Latimer et al. (2000) used a wedge model to indicate that by reducing the impact of side lobes, impedance inversion significantly increases resolution and decreases errors in the estimation of thickness. We therefore built an impedance model with sonic logs from nine wells and ran a model-based seismic inversion using commercial software. A 40-Hz Ricker wavelet was a good fit to wavelets extracted from the nine wells, and was used in the inversion. The initial model provides broader frequency content than band-limited seismic data and it compensates the data with low-frequency information (Russell and Lindseth, 1982; Russell, 1988). The inversion described in this paper uses the frequency content below 8 Hz — from the traveltime picks and log-based initial model — to compensate the band-limited seismic. Based on the linear relationship we found in our core analysis, we then interpreted the inverted impedance data for lithology and porosity.

Fractures are of great importance in microporous chert reservoirs because of their enhancement of permeability. Whereas fractures generally increase porosity by only 1% to 2%, they significantly reduce the strength of the rock and thereby reduce the seismic velocity (Thomson, 1986). Measurement of the effect of fractures on velocities was attempted, but results were not convincing. We noted signals from fractured core samples could be distorted, making it difficult to pick the first-arrival times, even though none of the observed fractures was throughgoing. Fermat's Principle dictates that a wave travels along a path that results in the shortest transit time; this principle requires the condition that energy bends around fractured zones in rock, which are the slower medium. For a core sample, the first-arrival times through the fractured and unfractured parts of the rock were indistinguishable. Nevertheless, the degree to which the fracture is sampled can be measured. Fractures are known to affect wave propagation at the seismic scale, and they can be measured in terms of traveltime thickness, incoherent scattering, and anisotropy (Thomson, 1986).

Although calibration of the effect of fractures on velocity measured on cores is not achievable, statistical relationships between seismic attributes and observations of fracture intensity in cores can be described. Three sets of geometric attributes were employed: (1) well-established coherence measures, (2) recently developed attributes of spectrally limited estimates of volumetric curvature, and (3) coherent-energy gradients (Figure 5). Estimation of coherence illuminates lateral changes in waveform and is an excellent indicator of faults and channels. Coherent-energy gradients permit measure-

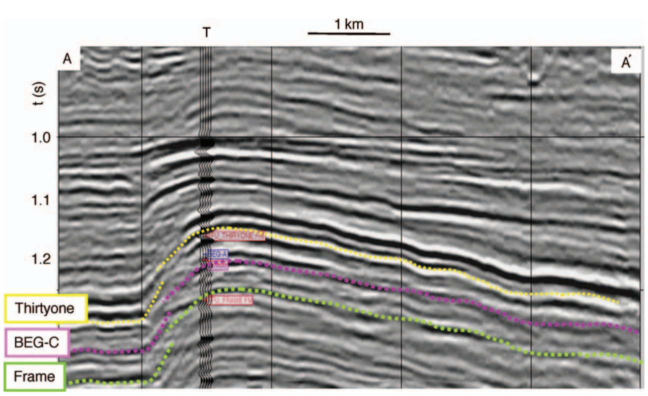

Figure 4. Seismic cross section AA′, through well "T" showing reversal of dip across axis of anticline. The Thirtyone Formation is bounded above by the yellow dotted marker and below by the green "Frame" marker. The BEG-C marker represents the top of the porous-chert interval.

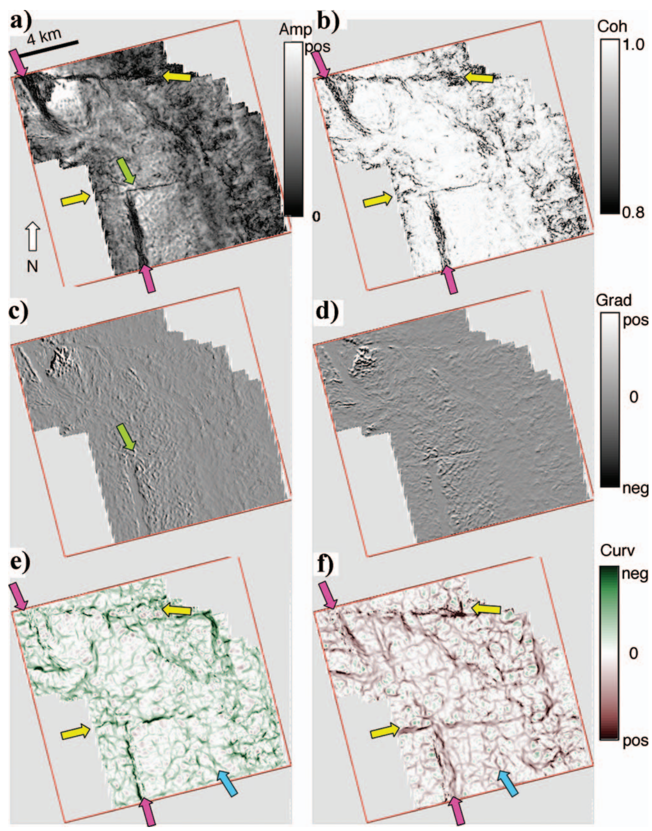

Figure 5. Horizon slices along the Devonian Thirtyone Formation through the following attribute volumes: (a) seismic amplitude, (b) coherence, (c) east-west component of the coherent, energy gradient, (d) north-south component of the coherent energy gradient, (e) most negative curvature; and (f) most positive curvature. Magenta arrows indicate major reverse faults; while yellow arrows indicate major strike-slip faults. Because these discontinuities are incoherent, they do not appear strongly in the coherent energy gradient volume. In contrast, the coherent energy gradient volume enhances lateral changes in thin-bed tuning, illuminating a subtle channel (green arrow) that is present, but difficult to see in the original amplitude. Green valleys and red ridges align with the major faults in the two curvature volumes shown in (e) and (f). However, a system of curvature lineaments also appears to the east of the producing area (indicated by the blue arrows) where the wells produce water. We suspect these lineaments represent subtle faults or fractures that reach deeper into water-filled formations.

ment of effects related to subtle lateral differences among thickness, lithology, fluid, and porosity. Dip, azimuth, curvature, and rotation of reflectors are measurements of reflector shape. The statistical relationship between curvature of strata and fractures is established (e.g., Lisle, 1994; Hart et al., 2002). These families of attributes are mathematically independent, but are coupled through underlying geologic relationships (Marfurt, 2006). Roberts (2001) introduced the concept of "most-negative curvature" (Figure 6) into structural geology. In the course of the research described here, volumetric estimates of most-negative curvature illuminated flexural lineaments believed to be associated with the geometry of fractures.

The attribute technology that was employed produces full 3D volumes that are calculated from seismic traces directly, with no requirement for preinterpreted horizons. This technology precludes unintentional bias and errors in selection of markers, which tend to be introduced during the process of interpretation (Blumentritt et al., 2006).

RESULTS

Laboratory measurements and fluid substitution

Four discrete lithofacies of the Thirtyone Formation were described by Ruppel and Barnaby (2001): limestone, thick-bedded chert, laminated chert, and brecciated chert. Rock properties of these lithofacies with various fluid contents were calculated by Gassmann's (1951) fluid-substitution method. Results indicate that lithology is the most important control of porosities and velocities (Figures 7 and 8). Among all lithofacies of the Thirtyone Formation, limestone has high grain density (2.71 g/cc) and the highest velocities. Among the chert lithofacies, laminated chert and mixed chert-carbonate lithofacies have low porosity and high velocity. Thick-bedded chert and massive chert are the more porous; at some localities porosity is more than 20%. In laminated cherts and carbonates, porosity generally is less than 5%; in limestone, porosity averages about 2%.

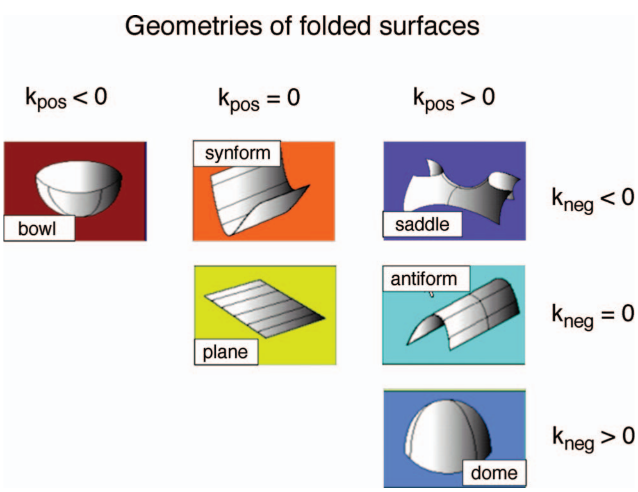

Figure 6. Classification of curvature in three dimensions. Note that values of the most-positive-curvature attribute can be negative and that values of most-negative curvature can be positive. Together, they define the shape of the reflector. (After Bergbauer et al., 2003.)

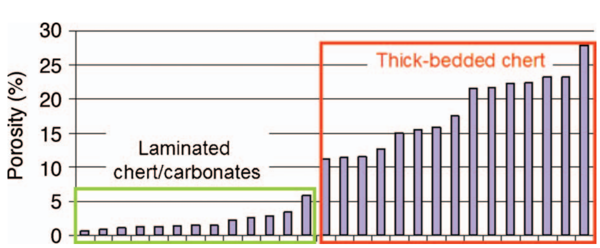

Figure 7. Porosity compared with lithofacies. The set of samples of thick-bedded chert indicates that porosity of this lithofacies exceeds 10%.

Porosity and velocity are strongly related. P- and S-wave velocities in porous chert are much slower than in limestone or thinly laminated cherts, which are less porous (Figures 9 and 10). The results of fluid substitution (Figures 9 and 10) indicate that fluid is less important in its effect on velocity than lithology or porosity. The measurements also indicate that velocity in water-saturated chert is similar to velocity published for water-saturated, consolidated sandstone (Han et al., 1986). However, at a given porosity, the velocity of chert is consistently greater than that of sandstone. The difference between velocities of chert and sandstone becomes larger with diminishing

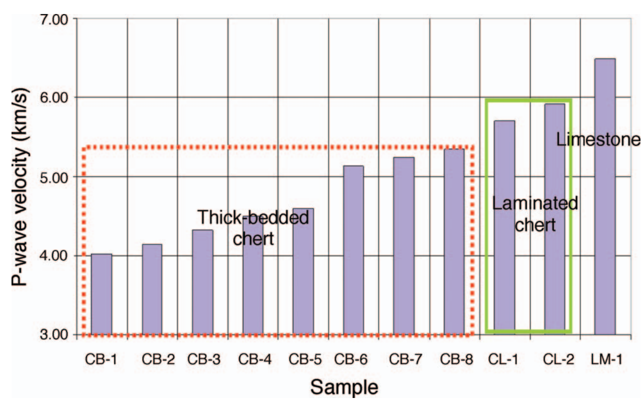

Figure 8. Relation between lithofacies and P-wave velocity. Laminated chert is composed of interbedded laminae of chert and limestone.

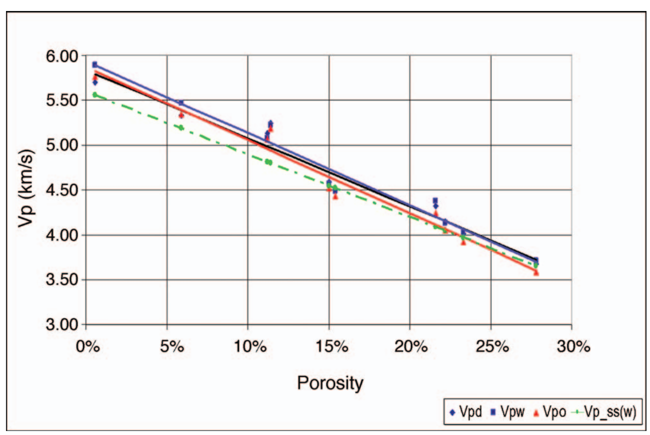

Figure 9. Linear relationship between porosity and P-wave velocity. Vpd, Vpw, and Vpo are velocities of dry chert, water-saturated chert, and oil-saturated chert, respectively. Vp_ss(w) is the empirical P-wave curve of water-saturated sandstone, (Han et al., 1986). Relationships: $Vpd = -7.6015\phi + 5.8388$, $R^2 = 0.9578$; $Vpw = -8.058\phi + 5.9408$, $R^2 = 0.9651$; $Vpo = -8.1564\phi + 5.8723$, $R^2 = 0.967$; $Vp\_ss(w) = -7\phi + 5.6$.

porosity, because the rock frame of chert is stiffer than that of sandstone. The Vp/Vs ratio is more sensitive to variation in fluid. The Vp/Vs ratio is greater in water-saturated rock than in oil-saturated or dry rock. The Vp/Vs ratio of dry rock is the smallest (Figure 11).

Impedance values based on the core measurements and fluid substitution were calculated. P- and S-wave impedance both indicate a direct relation to porosity (Figures 12 and 13). Although we did not have access to prestack or multicomponent data that would use the shear-wave measurements, we think the documentation of the sensitivity of shear wave to porosity is an important objective. Also, in different lithofacies impedance varies tremendously; the impedance of thick-bedded chert (the main reservoir) is much less than that of laminated chert and limestone (Figure 14).

Acoustic impedance inversion

Seismic data were inverted to generate a 3D acoustic-impedance volume. The impedance volume illuminates the distribution of porosity and lithology, laterally and vertically (Figures 15 and 16). An overlay of the original seismic data on the inversion results shows that the inversion helps illuminate a channel-like feature around well "Y" (Figure 17). The first 12 months of cumulative production was plotted, to correlate with impedance. All producing wells are in the area where impedances are low; in these areas porosities are high, as based on correlations derived in measurements of cores, fluid substitution, and from log data. Of course, production varied within the low-impedance area, which implies heterogeneity due to other factors, such as fractures.

Seismic attributes

Curvature of reflectors, coherence, and coherent-gradient volumes highlight subtle lineaments that are not seen, or that are difficult to detect in conventional seismic sections and time slices. Curvature is known to be correlated to fractures (Lisle, 1994; Hart et al., 2002; Melville et al., 2004). Orientations of lineaments observed in time slices through the chert reservoir interval were analized statisti-

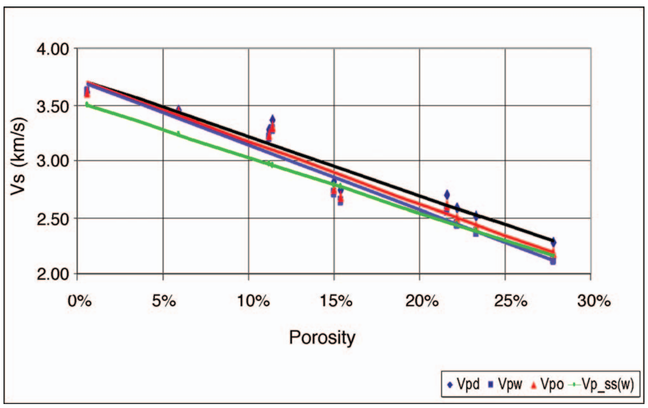

Figure 10. Linear relationships between porosity and S-wave velocity. Vsd, Vso, and Vsw are S-wave velocities of dry chert, oil-saturated chert, and water-saturated chert, respectively. Vs_ss(w) is the empirical S-wave curve for water-saturated sandstone (Han et al., 1986). Relationships: $Vsd = -5.2041\phi + 3.7331$, $R^2 = 0.9263$; $Vsw = -5.769\phi + 3.7224$, $R^2 = 0.9428$; $Vso = -5.55\phi + 3.7276$, $R^2 = 0.9369$; $Vs\_ss(w) = -4.91\phi + 3.52$.

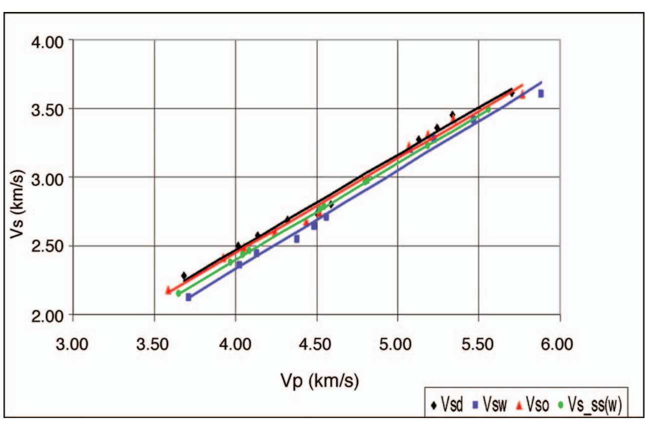

Figure 11. Linear relationships between P- and S-wave velocities. The Vp/Vs ratio varies with among fluids and with different saturations of a fluid. Vsd, Vso, and Vsw are S-wave velocities of dry chert, oil-saturated chert, and water-saturated chert, respectively. $Vpd = 0.6927Vsd - 0.3019$, $R^2 = 0.99$; $Vpw = 0.7204Vsw - 0.522$, $R^2 = 0.9893$; $Vpo = 0.6881Vpo - 0.3037$, $R^2 = 0.9908$; $Vp\_ss(w) = 0.7014Vs\_ss(w) - 0.408$ (Han et al., 1986).

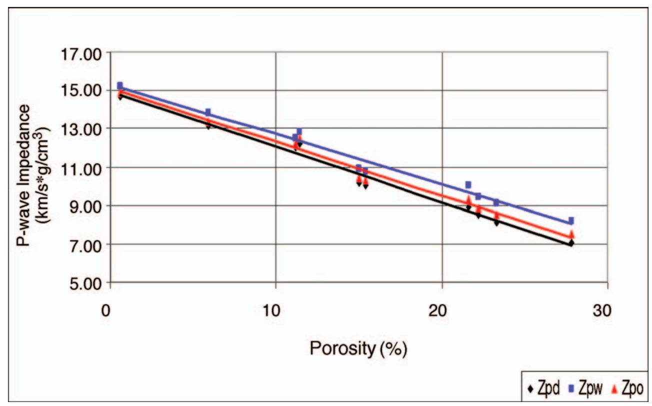

Figure 12. Relationship between porosity and P-wave (acoustic) impedance. The linear curves indicate that inverted impedance can be used to predict porosity, or porosity can be used to predict impedance. Zpd, Zpw, and Zpo are P-wave impedance of dry chert, water-saturated chert, and oil-saturated chert, respectively. $Zpd = -28.86\phi + 14.94$, $R^2 = 0.9838$; $Zpw = -26.226\phi + 15.327$, $R^2 = 0.9782$; $Zpo = -27.851\phi + 15.088$, $R^2 = 0.9826$.

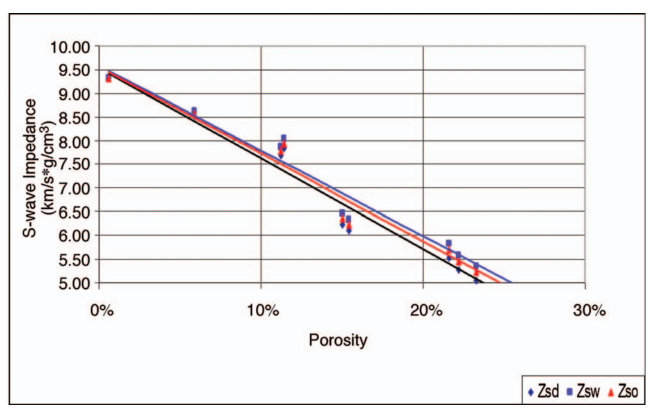

Figure 13. Relationship between porosity and S-wave impedance. Zsd, Zsw, and Zso are S-wave impedance of dry chert, water-saturated chert, and oil-saturated chert, respectively. $Zsd = -19.12\phi + 9.5428$, $R^2 = 0.9676$; $Zso = -18.445\phi + 9.5672$, $R^2 = 0.9644$; $Zsw = -17.984\phi + 9.5853$, $R^2 = 0.9619$.

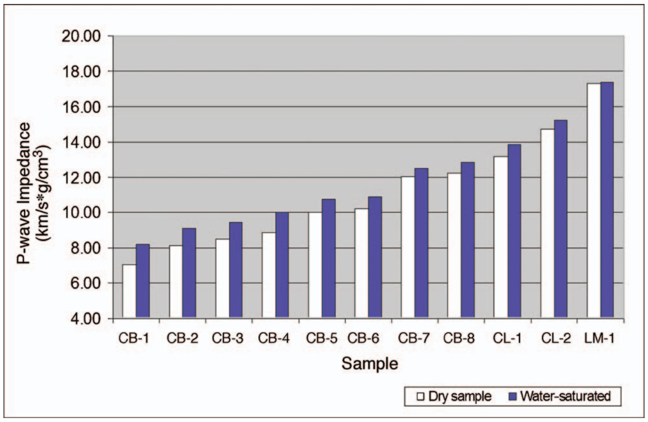

Figure 14. Relationship between (a) rock types, dry and water-saturated, and (b) P-wave impedance. CB, CL, and LM signify thick-bedded chert, laminated chert, and limestone. Clearly, the impedance of thick-bedded chert is much less than that of laminated chert or limestone.

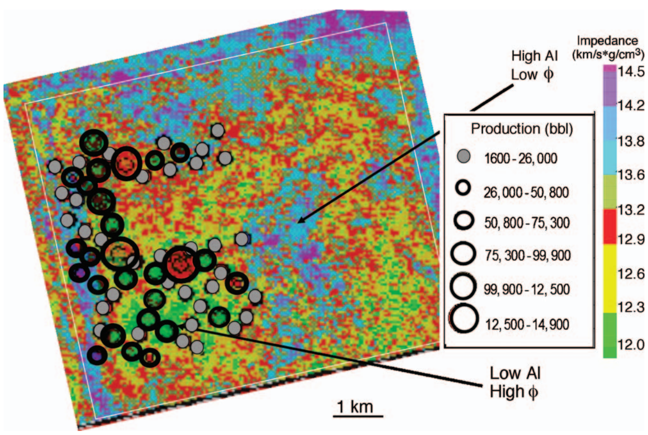

Figure 15. Average impedance beneath the BEG-C, a marker across the top of the lower pay interval of chert reservoirs (see Figure 4). Contours are time structure of the BEG-C marker. Distribution of low impedance and high porosity is illustrated. Distribution of impedance is an indicator of different lithofacies.

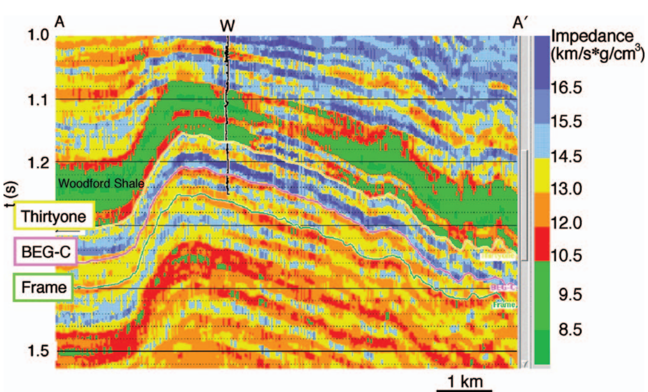

Figure 16. Cross-section AA′ (see Figures 2 and 14) through the seismic acoustic impedance volume. Cross-section shows evidence of low-impedance chert below the BEG-C marker, and shows the background Thirtyone Formation, which is high-impedance carbonate rock, dominantly limestone.

cally, and a rose diagram was constructed for structural analysis (Figure 18). Two sets of lineaments strike WNW and NNE. At least two large-offset, high-angle reverse faults are interpreted, on the western and eastern flanks of the anticline. A high-angle reverse fault is north of the University Waddell field. At least two stages of faulting are believed to have occurred. Paths favorable for breakthrough of water are oriented northeastward (personal communication,

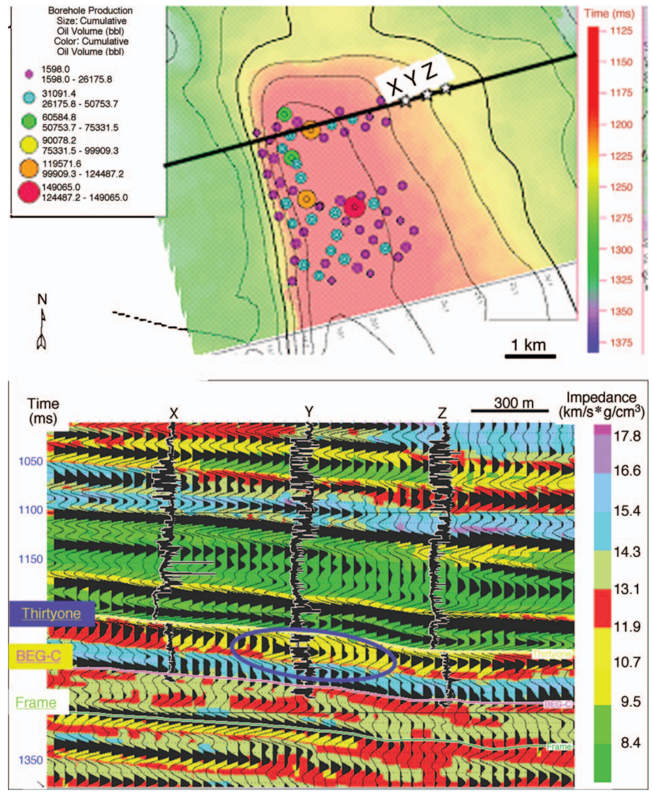

Figure 17. Comparison of original seismic data with results of inversion. Black traces are original seismic data; colored data are the inverted volume. Inversion results in more detail in the layers. Blue oval highlights a channel-form feature, delineated by impedance volume.

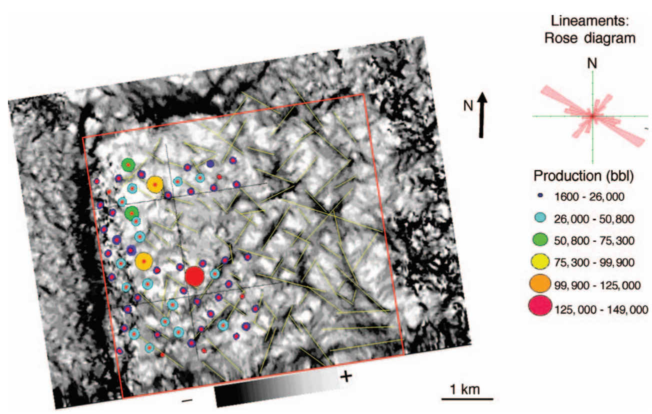

Figure 18. Time slice through the reservoir, from a most-negative-curvature volume generated from post-stack migrated seismic data. Azimuths of lineaments (yellow) are displayed in the rose diagram, according to relative frequencies. Bubbles depict cumulative production of each well, during first 12 months of production.

Schlumberger Oilfield Operating Services, 2003); they seem to not be related to zones of high porosity. If this northeastward trend is that of the tension fractures, a left-lateral coupling stress regime can be proposed as the fundamental mechanism, based on Sylvester's (1988) Simple Shear Model (Figure 19).

DISCUSSION

Because we compare velocities and impedance calculated from cores, logs, and seismic data, we are concerned with scaling. Results from our laboratory measurements and calculation using Gassmann's (1951) equation show evidence of good correlation with log-derived data (Figure 20). Furthermore, synthetic ties between logs and seismic are excellent. This fact validates the log-derived data, which formed the background geologic model for seismic-impedance inversion. Results of laboratory analyses show that chert of reservoir quality can be discriminated from carbonate rocks by its lower density (higher porosity) and lower velocity, which result in significantly lower impedance. Acoustic impedance works well in delineating the primary lithofacies, due to clear contrast between porous chert, tight, laminated chert, and limestone. However, results from fluid substitution using Gassmann's (1951) equation indicate that because of the stiff rock frame, oil and water in chert have similar impedance values; therefore, to differentiate between the fluids in chert is difficult. Thus the difference between oil and water can be neglected in differentiation of porosity from impedance, by using the relationship developed from the core measurements and fluid substitution. Given that acoustic impedance provides a direct measurement of porosity, various rock types can be classified, by reference to their impedance values. Seismic impedance volume delineates the distribution of porous lithofacies; it differentiates between chert lithofacies and between chert and carbonate rocks.

Seismic impedance illuminates the boundaries between strata and provides more geologic information than conventional seismic data. However, seismic impedance is altered where the reservoir is thinner than one-fourth the wavelength (Russell, 1988).

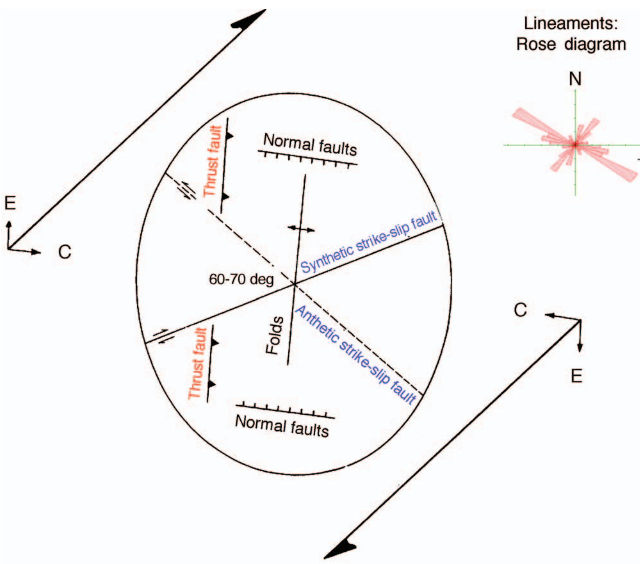

Figure 19. Interpretation of lineaments. The diagram is modified from Sylvester's (1988) structural model for fractures/faults, folds, and their relations under a certain stress regime. Coupling of regional stress can be decomposed into compressional stress (C) and extensional stress (E), which produce fractures/faults and folds.

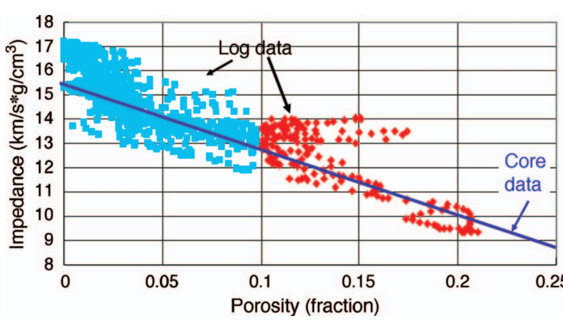

Figure 20. Relation of porosity and impedance, from core data and log data. All dots are measurements from well-log data. Blue dots are samples with porosity of less than 10%; red dots are samples with porosity equal to or more than 10%. The blue line was derived from core samples, water-saturated, for comparison with the log-derived porosity data.

CONCLUSIONS

In this paper, we share some of our initial work in using core, petrophysical-log, and rock-physics data to calibrate impedance inversion and seismic attributes for the characterization of interwell distribution of porosity and fracture zones in an unconventional but important reservoir rock — the Devonian cherts of the Central Basin Platform in west Texas. To our knowledge, this is the first published measurement of chert rock properties. A simple but accurate linear relationship is established between porosity and P-wave velocity and between porosity and P- and S-wave impedances.

Preliminary analysis shows evidence of qualitative correlation between curvature of reflectors and production of petroleum. However, at some localities in the University Waddell field where rocks are fractured, the fractures do not contribute constructively to production of oil and gas. Some highly productive wells are in areas with few pronounced lineaments or are in areas where strata show evidence of low-negative or high-positive curvature. Cores from the University Waddell field show that thick-bedded chert is fractured less than laminated chert and limestone are fractured. At the field scale, pronounced fractures may penetrate to free water below the oil-water contact. We suspect that this may be the case at the University Waddell field. If so, then this hypothesis would explain why wells that produce the most petroleum are on the crest and western flank of the anticline — where fractures are comparatively small — whereas wells that produce greater quantities of water are in areas where lineaments are more evident.

ACKNOWLEDGMENTS

This work was supported by the State of Texas Advanced Technology Grant 003652-0321-2001 and the sponsors of the Allied Geophysical Lab (AGL), University of Houston. We are most grateful to Professor De-Hua Han for his help, guidance, and for the use of his facilities and methods at the University of Houston Rock Physics Laboratory. We are grateful for the guidance of Al Lacazette of naturalfractures.com for advice on the study of fractures in cores. We thank Burlington Resources, Schlumberger Oilfield Services, and Steve Ruppel and others at the Bureau of Economic Geology (BEG) for data and insight. Finally, we thank Hampson Russell and Geoquest for providing the University of Houston with royalty-free copies of Strata and Geoframe for educational and research purposes.

REFERENCES

Batzle, M. L., and Z.-J. Wang, 1992, Seismic properties of pore fluids: Geophysics, **57**, 1396–1408.
Bergbauer, S., T. Mukerji, and P. Hennings, 2003, Improving curvature analyses of deformed horizons using scale-dependent filtering techniques: AAPG, **87**, 1255–1272.
Blumentritt, C. H., K. J. Marfurt, and E. C. Sullivan, 2006, Volume based curvature attributes illuminate fracture orientations, Lower Mid Paleozoic, Central Basin platform, West Texas: Submitted to Geophysics.
Gassmann, F., 1951, Über die Elastizität poroser Medien: Veirteljahrsschrift der Naturforschenden Gesellschaft in Zürich, **96**, 1–23.
Han, D. H., A. Nur, and D. Morgan, 1986, Effects of porosity and clay content on wave velocities in sandstones: Geophysics, **51**, 2093–2107.
Hart, B. S., R. Pearson, and G. C. Rawling, 2002, 3-D seismic horizon-based approaches to fracture-swarm sweet spot definition in tight-gas reservoirs: The Leading Edge, **21**, 28–35.
Hughes, D. S., and H. J. Jones, 1950, Variation of elastic moduli of igneous rocks with pressure and temperature: Bulletin of Geological Society of America, **61**, 843–856.
Kalkomey, C. T., 1997, Potential risks when using seismic attributes as predictors of reservoir properties: The Leading Edge, **16**, 247–251.
Kallweit, R. S., and L. C. Wood, 1982, The limits of resolution of zero-phase wavelets: Geophysics, **47**, 1035–1046.
Latimer, R. B., R. Davidson, and P. V. Riel, 2000, An interpreter's guide to understanding and working with seismic-derived acoustic impedance data: The Leading Edge, **19**, 242–256.
Lisle, R. J., 1994, Detection of zones of abnormal strains in structures using Gaussian curvature analysis: AAPG Bulletin, **79**, 1811–1819.
Marfurt, K. J., R. L., Kirlin, S. L. Farmer, and M. S. Bahorich, 1998, 3-D seismic attributes using a semblance-based coherency algorithm: Geophysics, **63**, 1150–1165.
Marfurt, K. J., 2006, Robust estimates of reflector dip and azimuth: Accepted by Geophysics, December, 2005.
Melville, P., O. al Jeelani, S. al Menhali, and J. Grotsch, 2004, Three-dimensional seismic analysis in the characterization of a giant carbonate field, onshore Abu Dhabi, United Arab Emirates, *in* G. P. Eberli, J. L. Masaferro, and J. F. Sarg, (eds.), Seismic imaging of carbonate reservoirs and systems: AAPG Memoir, **81**, 123–148.
Roberts, A., 2001, Curvature attributes and their application to 3D interpreted horizons: First Break, **19**, 85–100.
Rogers, J. P., and M. W. Longman, 2001, An introduction to chert reservoirs in North America: AAPG Bulletin, **85**, 1–5.
Ruppel, S. C., and R. J. Barnaby, 2001, Contrasting styles of reservoir development in proximal and distal chert facies: Devonian Thirtyone Formation, Texas: AAPG Bulletin, **85**, 7–33.
Ruppel, S. C., and S. D. Hovorka, 1995, Controls on reservoir development in Devonian chert: Permian Basin, Texas: AAPG Bulletin, **79**, 1757–1785.
Russell, B. H., 1988, Introduction to seismic inversion methods: Course Notes Series, **2**, SEG.
Russell, B. H., and R. O. Lindseth, 1982, The information content of synthetic sonic logs — A frequency domain approach: Presented at the 1982 convention of the EAEG.
Sears, F. M., and B. P. Bonner, 1981, Ultrasonic attenuation measurement by spectral ratios utilizing signal processing techniques: IEEE Transactions on Geoscience and Remote Sensing, GE19, 95–99.
Sylvester, A. G., 1988, Strike slip faults: Geological Society of American Bulletin, **100**, 1666–1703.
Thomson, L., 1986, Weak elastic anisotropy: Geophysics, **51**, 1954–1966.